Rad-NeRF: Ray-decoupled Training of Neural Radiance Field

Lidong Guo[1*] **Xuefei Ning**[1*†] **Yonggan Fu**[2] **Tianchen Zhao**[1]

Zhuoliang Kang[3] **Jincheng Yu**[1] **Yingyan (Celine) Lin**[2] **Yu Wang**[1†]

[1]Tsinghua University [2]Georgia Institute of Technology [3]Meituan

Abstract

Although the neural radiance field (NeRF) exhibits high-fidelity visualization on the rendering task, it still suffers from rendering defects, especially in complex scenes. In this paper, we delve into the reason for the unsatisfactory performance and conjecture that it comes from interference in the training process. Due to occlusions in complex scenes, a 3D point may be invisible to some rays. On such a point, training with those rays that do not contain valid information about the point might interfere with the NeRF training. Based on the above intuition, we decouple the training process of NeRF in the ray dimension softly and propose a **Ra**y-**d**ecoupled Training Framework for neural rendering **(Rad-NeRF)**. Specifically, we construct an ensemble of sub-NeRFs and train a soft gate module to assign the gating scores to these sub-NeRFs based on specific rays. The gate module is jointly optimized with the sub-NeRF ensemble to learn the preference of sub-NeRFs for different rays automatically. Furthermore, we introduce depth-based mutual learning to enhance the rendering consistency among multiple sub-NeRFs and mitigate the depth ambiguity. Experiments on five datasets demonstrate that Rad-NeRF can enhance the rendering performance across a wide range of scene types compared with existing single-NeRF and multi-NeRF methods. With only 0.2% extra parameters, Rad-NeRF improves rendering performance by up to 1.5dB. Code is available at https://github.com/thu-nics/Rad-NeRF.

1 Introduction

Novel view synthesis is an important task within the domains of computer vision and computer graphics, playing an essential role in a variety of applications, such as autonomous driving, augmented reality, and so on. Recently, Neural Radiance Field (NeRF) [17] has emerged as a promising solution, achieving high-fidelity visualizations on the novel view synthesis task. It implicitly encodes 3D scenes through neural networks and trains the networks using volume rendering.

Despite NeRF's excellent scene representation ability, it still suffers from rendering defects when dealing with complex scenes, such as 360-degree unbounded scenes [37, 2] and large scenes with free shooting trajectories [30, 27, 26]. One of the main reasons is the limited model capacity. However, directly increasing the network's size yields marginal performance improvement [18].

Our fundamental intuition is that the training interference from invisible rays affects NeRF's performance. Let us consider a simple case of a 360-degree unbounded scene with a central object

*Both authors contribute equally to this work.

†Corresponding authors: Xuefei Ning (foxdoraame@gmail.com), Yu Wang (yu-wang@tsinghua.edu.cn).

38th Conference on Neural Information Processing Systems (NeurIPS 2024).

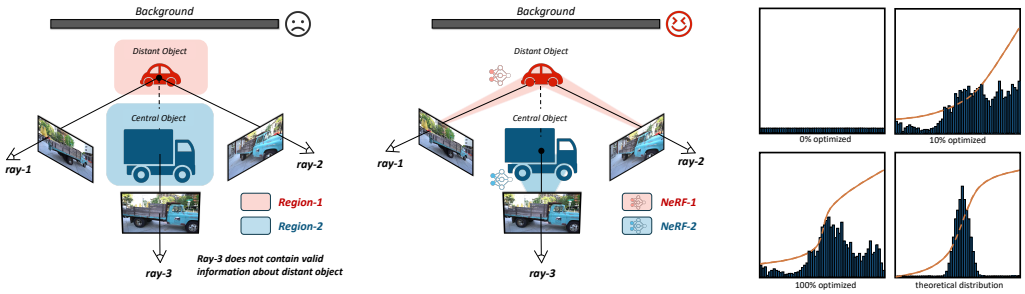

(a) Training interference caused by occlusions (b) Decouple training in the ray dimension (Ours) (c) Inaccurate sampling of ray-3

Figure 1: A case in 360-degree unbounded scenes (bird-eye view). (a) For the distant object, invisible ray-3 interferes with ray-1/2 training. (b) The ray-based multi-NeRF framework considers variable visibility of objects to different rays and decouples training in the ray dimension. (c) Compared to the theoretical weight distribution, the sampling along ray-3 is inaccurate incurring training interference.

(truck) and a distant object (car). As illustrated in Figure 1(a), a 3D point located on the distant object can be observed from ray-1 and ray-2, but is invisible to ray-3 due to the occlusion presented by the central object. Although NeRF models transmittance in its volume rendering formula, it exhibits low geometric modeling accuracy and inaccurate sampling distribution in complex scenes, especially at the start of training, as Figure 1(c) shows. So, 3D points on the distant object might be sampled by the ray-3, and the model is trained on these points by the ray-3 color. However, ray-3 does not contain any meaningful information about the distant object, potentially interfering with the NeRF's training. In contrast, considering the different visibility of the object to different rays, our intuition is that rather than using one NeRF, assigning the rays terminating at the distant object to NeRF-1 and the rays terminating at the central object to NeRF-2 could be better, as shown in Figure 1(b).

To verify the above intuition, we manually select two sets of images in the TAT dataset[13]. One set contains 80 images of the train's front side, while the other set includes the former set and 80 backside images. We train two NeRFs using these two sets respectively. As shown in Figure 2, the model trained on the mixed set performs worse on the front side, which matches our intuition.

To mitigate the training interference caused by invisible rays, the intuition solution is to decouple the training of the rays terminating at different regions. To this end, we propose a **ray-decoupled training framework for neural rendering (Rad-NeRF)**. Within the Rad-NeRF framework, an ensemble of sub-NeRFs has different preferences for different rays through a gate module. With the help of the gate module, sub-NeRFs' outputs are fused by post-volume-rendering fusion to yield final rendering results. Notably, the gate module is jointly optimized with NeRF, allowing it to automatically learn the preference of each sub-NeRF for various rays in an end-to-end manner. This **learnable gating** design makes Rad-NeRF generally applicable to diverse scenes, which stands in contrast to prior multi-NeRF methods [27, 26] that rely on manually defined allocation rules.

Additionally, we design a depth-based mutual learning method for the multi-NeRF framework to ensure the rendering consistency among multiple sub-NeRFs. In addition to learning colors, sub-NeRFs teach each other with their rendered depths. Traditional NeRF methods may struggle with generalization to novel views despite accurately rendering training views, as they often fail to capture precise geometry [7, 37]. In contrast, our depth-based mutual learning approach serves as a form of geometric regularization, alleviating the depth ambiguity and avoiding overfitting.

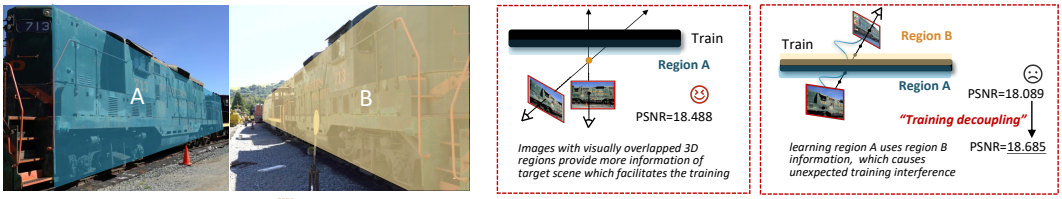

Without training interference Decoupling mitigates training interference

Figure 2: Oracle experiment: Training interference from invisible rays affects NeRF's performance.

To verify the effectiveness of Rad-NeRF, we conduct extensive experiments on various types of datasets. The results show that Rad-NeRF can exhibit *anti-aliasing effects* and obtain *superior geometry modeling*, thus consistently improving the rendering quality of novel views. In addition, Rad-NeRF is *parameter-efficient* and *super simple to implement*. With only 0.2% extra parameters, Rad-NeRF can increase rendering performance by up to 1.5dB compared to Instant-NGP. By scaling the number of sub-NeRFs through ray-wise decoupling, Rad-NeRF achieves better performance-to-parameter scalability than scaling other dimensions, such as the MLP width or the feature grid.

2 Related Work

2.1 Neural Radiance Field

Neural Radiance Field (NeRF) [17] has received much attention since it was proposed. It uses MLPs to implicitly represent 3D objects or scenes, achieving realistic rendering results. There have been intensive studies on NeRF's extension, including increasing NeRF's training/inference efficiency [36, 8, 21, 25, 18, 5], applying NeRF to specific scenes (large/unbounded/poor-textured) [15, 37, 2, 31, 26, 27, 38], applying NeRF to other tasks (surface reconstruction/scene editing) [35, 20, 29, 14, 33, 32], increasing NeRF rendering quality in few-shot setting [10, 12, 19, 7]. In this work, we aim to increase NeRF's rendering quality in complex scenes, and propose a multi-NeRF training framework, which can leverage the techniques proposed by these single-NeRF researches.

2.2 Multi-NeRF Representation

Due to the limited model capacity, the multi-NeRF method is widely adopted to improve the rendering quality, which can be categorized into point- and ray-based multi-NeRF methods.

Point-based multi-NeRF method. These methods divide the 3D space in the point-dimension [30, 37, 38]. 3D points in different regions are computed by different sub-NeRFs. For example, NeRF++ [37] proposes the sphere inversion transformation to map an infinite space to a bounded sphere first, and it uses two NeRFs to model the foreground and background regions respectively. Switch-NeRF [38] also partitions the scenes in the point-dimension. These methods do not consider the different visibility of a target region to different views and cause training interference on complex scenes with many occlusions. For example, the front side of an object is not visible when it is observed from the back view or blocked by an occlusion. Training the sub-NeRF with rays that do not contain any valid information about the target region might interfere with the training.

Ray-based multi-NeRF methods. These methods allocate training rays to different sub-NeRFs and train sub-NeRFs independently. Block-NeRF [26] and Mega-NeRF [27] perform the ray allocation in the image-granularity and pixel-granularity, respectively. Both of them need a manually defined allocation rule, which requires prior scene knowledge and cannot be easily adapted to other types of scenes. The former work trains sub-NeRFs in large-scale road scenes with prior knowledge of the image shooting position distribution, and the latter one trains sub-NeRFs in open drone scenes and allocates the rays based on the ray intersecting positions with a horizontal plane. However, defining a ray allocation rule for complex scenes lacking prior scene-specific knowledge remains challenging. Another related work is NID [28], which proposes a mixture-of-experts NeRF for generalizable scene modeling. In this work, different experts serve as the basis to construct the implicit field of different scenes and the gating module takes in the new scene's image as the input (i.e., image-granularity).

In this work, we propose a gate-guided multi-NeRF mutual learning framework, performing the allocation and decoupling the training in the ray dimension softly. Compared to other multi-NeRF methods, Rad-NeRF boosts the rendering quality without the need for prior scene knowledge.

3 Preliminary

NeRF [17] uses neural networks to represent 3D scenes implicitly. Two MLPs model the density and color of spatial points respectively. The input of density MLP F_σ is the 3D point coordinate $\mathbf{x}$. The input of color MLP F_c includes view direction θ and feature f output by density MLP. NeRF proposes the volume rendering method to render each pixel of an image. It samples N points along

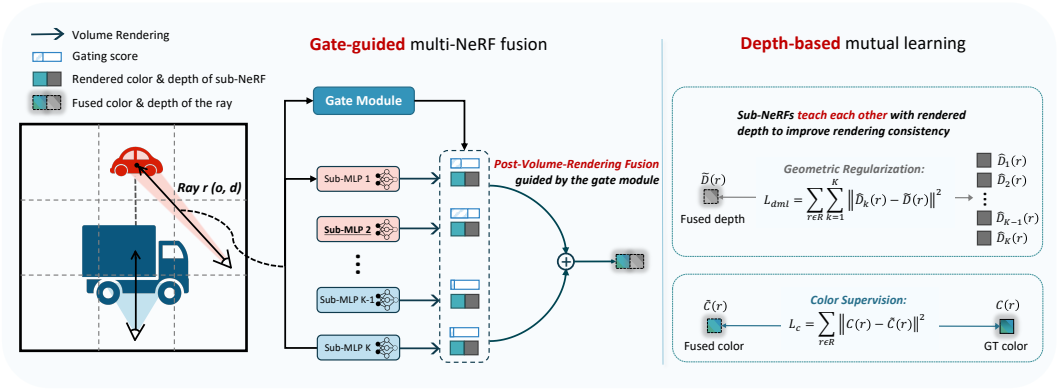

Figure 3: The overview of Rad-NeRF. We construct a multi-NeRF framework based on the hybrid representation, where the feature grid is shared for all sub-NeRFs and the MLP decoders are independent. **(Left)** Given a ray, the soft gate module encodes the ray's data and outputs a soft score. Then, guided by the gating score, sub-NeRFs' outputs are fused after the volume rendering process. **(Right)** The fused rendered depth of the ray is used to regularize each sub-NeRF's geometric encoding.

the ray and renders the pixel's color $\hat{C}(\mathbf{r})$ by discretely summing density σ_i and color $\mathbf{c}_i$ of each point i, which approximates the integral $C(\mathbf{r})$ as follows:

$$C(\mathbf{r}) = \int_0^{+\infty} w(t)\mathbf{c}(t)dt \quad \hat{C}(\mathbf{r}) = \sum_{i=1}^{N} w_i \mathbf{c}_i, \tag{1}$$

$$T_i = \exp\left(-\sum_{j=1}^{i-1} \sigma_j \delta_j\right) \quad w_i = T_i\left(1 - e^{-\delta_i \sigma_i}\right), \tag{2}$$

where t_i is the distance between i-th sample's position and the starting point of the ray, $\delta_i = t_{i+1} - t_i$ is the distance between adjacent samples and T_i represents the probability that the ray travels from the start to point i without hitting. The NeRF optimization is based on color supervision.

4 Rad-NeRF

NeRF faces the challenge of limited model capacity when rendering complex scenes [37, 30, 38]. However, directly increasing the number of model parameters yields marginal improvement in the rendering quality [18], posing an important research question: "how to effectively scale up the capacity of NeRF". While the multi-NeRF methods have been proposed as an effective technique in response to this question, they still face limitations in handling complex scenes (with many occlusions and arbitrary shooting trajectories) due to training interference among invisible rays. In this work, we propose a ray-decoupled training framework (Rad-NeRF), effectively scaling up model's capacity by decoupling training in the ray dimension in a learnable way. Figure 3 gives an overview of Rad-NeRF.

4.1 Gate-guided Multi-NeRF Fusion

Motivated by the intuition and oracle experiment discussed in Section 1, rather than using a single NeRF model, designing a multi-NeRF structure that considers different visibility of the region to different rays and decouple NeRF's training in the ray-dimension could be better. We design a ray-based multi-NeRF model structure and introduce a soft gate module to learn the preference of each sub-NeRF for various rays in a learnable way.

Multi-NeRF Structure. As shown in Figure 3, we employ a shared feature grid among sub-NeRFs and keep MLP decoders independent for the multi-NeRF structure. As different rays may pass through the same region of 3D space, weight sharing for the feature grid helps training, owing to the feature grid's responsibility for encoding features of 3D spatial points. As validated by the Oracle experiment, training with regions A and B facilitates the training of the shared feature grid

and improves the rendering quality(PSNR 18.685 vs 18.488). Meanwhile, as the MLP decoder is designed to encode view information, constructing an ensemble of independent MLP decoders helps to decouple the training in the ray dimension, and thus maintains the preference of sub-NeRFs for various rays. Additionally, such structure is a multi-model extension of Instant-NGP [18], helping to avoid a significant increase in the number of parameters and training complexity. The hybrid representation also maintains high training efficiency.

Soft Gate Module. We incorporate a soft gate module to assign gating scores to the sub-NeRFs for each ray. The soft gate module is jointly optimized with NeRF, enabling it to learn the preference of each sub-NeRF for different rays in an end-to-end manner. In contrast to manually assigning training rays to sub-NeRFs, this learnable gating design makes Rad-NeRF **generally applicable to diverse scenes lacking prior scene-specific knowledge**. In Section 5.2, we will also show that the gate module can learn to assign reasonable gating scores that reflect the object visibility of rays, aligning with our intuition that decoupling training in the ray-dimension is important.

Specifically, we employ a four-layer MLP followed by a Softmax function as the gate module. The gate module takes the starting point and direction (o,d) of a ray $\mathbf{r}$ as the input, and outputs the gating scores $\boldsymbol{G}(\mathbf{r})$ of multiple sub-NeRFs associated with this ray. Instead of applying any sparsification strategies on the gating score $\boldsymbol{G}(\mathbf{r})$ as in previous work [38], such as top-k gating function [23], we use soft gating scores to enhance the smoothness and consistency of rendered results.

As discussed in Section 3, each ray corresponds to a pixel on the image. Following the volume rendering process, we can obtain K rendered colors for each ray, where K is the number of sub-NeRFs. Subsequently, multi-NeRFs' outputs are fused in a post-volume-rendering ordering to obtain the final rendering results. The fused color $\tilde{C}(\mathbf{r})$ of the ray $\mathbf{r}$ can be written as below:

$$\tilde{C}(\mathbf{r}) = \sum_{k=1}^{K} G_k(\mathbf{r})\hat{C}_k(\mathbf{r}), \tag{3}$$

where $G_k(\mathbf{r})$ is the k-th element of gating score $\boldsymbol{G}(\mathbf{r})$ and $\hat{C}_k(\mathbf{r})$ is the rendered color of k-th sub-NeRF for the ray $\mathbf{r}$.

4.2 Depth-based Mutual Learning

By the learnable soft gating design, different sub-NeRFs learn different encodings of the scene. We introduce a mutual learning method to enhance the rendering consistency and robustness of sub-NeRFs, wherein each sub-NeRF not only learns from ground truth but also learns from each other. Due to the lack of the ground truth for per-ray depth, NeRF may fail to learn accurate geometry despite accurately rendering training views, which adversely affects its generalization to novel views. To address this, we perform mutual learning with the rendered depths of sub-NeRFs, which serves as a form of geometric regularization and helps the model find more robust geometric solutions. The per-ray depth estimation $\hat{D}(\mathbf{r})$ can be written as Equation 4, where t_i is the i-th sample's distance from the starting point on the ray.

$$\hat{D}(\mathbf{r}) = \sum_{i=1}^{N} w_i t_i, \tag{4}$$

In practice, we first fuse the rendered depths of sub-NeRFs guided by the gating score $\boldsymbol{G}(\mathbf{r})$. Then we use L2 distance to quantify the match of each sub-NeRF's rendered depth $\hat{D}_k(\mathbf{r})$ and the fused depth $\tilde{D}(\mathbf{r})$. Our depth-based mutual learning loss is defined as below, where $\mathcal{R}$ is the set of sampled rays:

$$L_{dml} = \sum_{\mathbf{r}\in\mathcal{R}} \sum_{k=1}^{n} \|\hat{D}_k(\mathbf{r}) - \tilde{D}(\mathbf{r})\|^2, \tag{5}$$

Compared to directly averaging multiple sub-NeRFs' depth predictions, the gate-guided fused depth $\tilde{D}(\mathbf{r})$ is more accurate, as the gating score $\boldsymbol{G}(\mathbf{r})$ can reflect the prediction confidence of each sub-NeRF for the ray $\mathbf{r}$.

Table 1: Quantitative results in complex scenes.

Methods	TAT			NeRF-360-v2			Free-Dataset		
	PSNR↑	SSIM↑	LPIPS↓	PSNR↑	SSIM↑	LPIPS↓	PSNR↑	SSIM↑	LPIPS↓
NeRF++	20.419	0.663	0.451	27.211	0.728	0.344	24.592	0.648	0.467
MipNeRF360	**22.061**	**0.731**	**0.357**	**28.727**	**0.799**	**0.255**	**27.008**	**0.766**	0.295
MipNeRF360$_{short}$*	20.078	0.617	0.508	25.484	0.631	0.452	24.711	0.648	0.466
DVGO	19.750	0.634	0.498	25.543	0.679	0.380	23.485	0.633	0.479
Instant-NGP	20.722	0.657	0.417	27.309	0.756	0.316	25.951	0.711	0.312
F2-NeRF	–	–	–	26.393	0.746	0.361	26.320	**0.779**	**0.276**
Switch-NGP†	20.512	0.654	0.432	26.524	0.740	0.331	25.755	0.694	0.341
Block-NGP†	20.783	0.659	0.415	27.436	0.761	0.298	26.015	0.702	0.325
Rad-NeRF	**21.708**	**0.672**	**0.398**	**27.871**	**0.769**	**0.298**	**26.449**	0.719	**0.285**

* MipNeRF360 requires nearly one day for training. For a fair comparison, we also report its results with one-hour of training.
† We adapt Switch-NeRF and Block-NeRF to the Instant-NGP fast training framework.

4.3 The Overall Training Loss

The overall loss function of Rad-NeRF is given by:

$$L = L_c + \lambda_1 L_{dml} + \lambda_2 L_{cv}, \tag{6}$$

where $L_c = \sum_{\mathbf{r}\in\mathcal{R}} \|C(\mathbf{r}) - \tilde{C}(\mathbf{r})\|^2$ ($C(\mathbf{r})$ is the ground truth color value of ray $\mathbf{r}$) is the rendering loss. λ_1 and λ_2 are the weights for regularization terms, which are the only hyper-parameters to be set. The value of λ_1 is chosen from 1×10^{-4} and 5×10^{-3}. λ_2 is set to 1×10^{-2} on all the datasets. L_{cv} is the balancing regularization on the Coefficient of Variation of the soft gating scores, which prevents the gate module from collapsing onto a specific sub-NeRF. The details of L_{cv} are described and discussed in the Appendix B.

5 Experiments

5.1 Datasets and Baselines

Datasets. We use five datasets from different types of scenes to evaluate our Rad-NeRF. (1) Object dataset: we take *Masked Tanks-And-Temples dataset (MaskTAT)* [13] for evaluation, which are photographed objects with masked background; (2) 360-degree inward/outward-facing datasets: we take *Tanks-And-Temples (TAT) dataset* with unmasked background [13] and *NeRF-360-v2 dataset* [2] to evaluate on scenes with large dynamic depth range; (3) free shooting-trajectory datasets: we conduct experiments on *Free-Dataset [30]* and *ScanNet dataset* [6], which are large outdoor and indoor scenes respectively. Both larger view ranges and more irregular shooting trajectories pose greater challenges for NeRF rendering.

Baselines. We compare our Rad-NeRF with two types of methods: one type uses the grid-based NeRF framework as we do, including PlenOctrees [36], DVGO [25], Instant-NGP [18] and F2-NeRF [30]. The other one is the MLP-based NeRF method, including NeRF [17], NeRF++ [37], MipNeRF [1] and MipNeRF360 [2], which is inefficient in training and needs almost one day for training in complex scenes. Note that we also implement the NGP-version of Block-NeRF [26], Switch-NeRF [38] and Mega-NeRF [27] to validate the superiority of Rad-NeRF to other multi-NeRF methods. The implementation details of Mega-NGP are shown in the Appendix F.

5.2 Comparative Studies

Rad-NeRF achieves higher rendering quality than existing single- and multi-NeRF methods. We report the main quantitative results on the complex scenes and the object dataset in Table 1 and Appendix D respectively. Within no more than one hour of training, Rad-NeRF achieves higher rendering quality compared to other fast training methods and multi-NeRF methods, including Switch-NGP and Block-NGP. We can also see that while Rad-NeRF is designed for complex scene

Figure 4: Qualitative comparisons on three complex scenes. Rad-NeRF achieves better recovery of details for distant objects and less textured regions such as the wall. (Zoom in for the details, e.g., sky, banister, roadblock, wall.)

rendering, it can also improve the rendering performance of objects. We also integrate Rad-NeRF with the recent SOTA single-NeRF framework ZipNeRF [3], named Rad-ZipNeRF, in the Appendix I. Rad-ZipNeRF obtains better rendering performance, validating Rad-NeRF's potential for integration with different frameworks.

Rad-NeRF achieves better recovery of distant details and accurate rendering for less textured regions. The qualitative results are shown in Figure 4. Compared to other methods, Rad-NeRF achieves better rendering quality in both outdoor and indoor scenes. In outdoor scenes, Rad-NeRF produces detailed and realistic rendering results for the sky and other distant objects. In indoor scenes, Rad-NeRF generates more accurate details for less textured regions such as the wall. Rad-NeRF takes advantage of the gate-guided training decoupling in the ray dimension to boost the model's performance effectively. Results on the ScanNet dataset are shown in the Appendix C.

The gate module learns to reasonably assign gating scores. We visualize how the gate module performs training decoupling in Figure 5. As the two sub-NeRFs exhibit complementary gating scores, we omit sub-NeRF2's visualization for brevity. (1) In the Truck scene, the gate module assigns different preferences to sub-NeRF1 in foreground/background regions, thereby mitigating the interference from foreground rays on sub-NeRF1's training with the background region. (2) In the Train scene, sub-NeRF1 exhibits higher preferences for the back side, thereby mitigating the

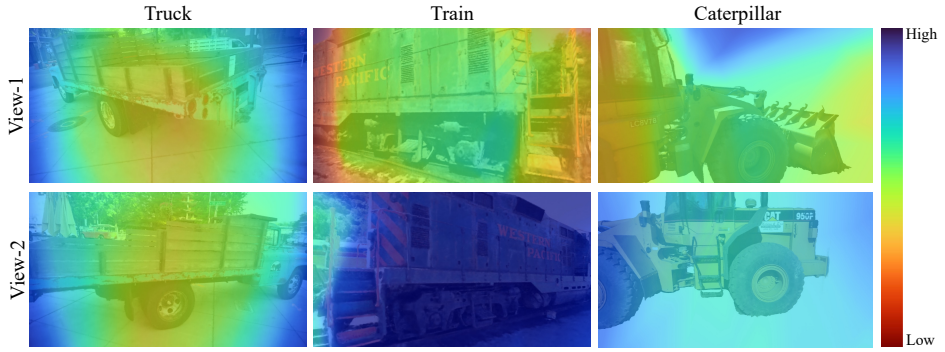

Figure 5: Visualization of the gating scores of sub-NeRF1 on two different views (visualization of sub-NeRF2 is omitted for brevity).

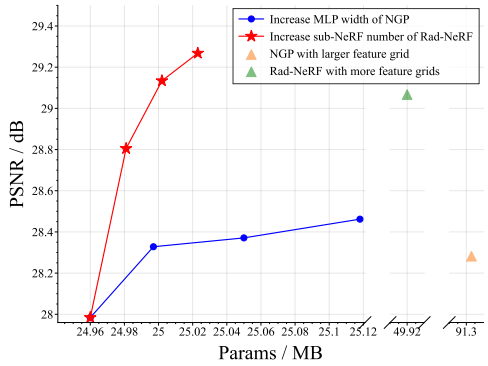

Figure 6: Scalability study of Rad-NeRF.

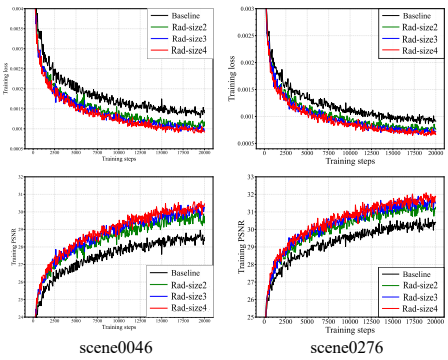

Figure 7: Convergence curve on ScanNet.

training interference from invisible frontside rays. (3) In the Caterpillar scene, the gating module assigns different preferences to foreground/background regions or the different sides of the caterpillar, which are clearly distinguished. The visualization demonstrates that Rad-NeRF learns reasonable ray allocations, matching our intuition. Besides, we observe that in some specific scenes, such as the Truck scene, the gating score visualization indeed shows a significant difference between the edge and the central region, correlating with the aliasing issue. Such observation illustrates that tackling the aliasing issue in some scenarios is another insightful explanation of the Rad-NeRF's effectiveness, which is supplementary to our original motivation targeting scenarios with heavy occlusions.

Scaling up NeRF with the Rad-NeRF framework is more effective than scaling the MLP width, increasing the feature grid size, or adding more feature grids. By default, we set the number of sub-NeRFs to 2 in all experiments. As shown in Figure 6, when the number of sub-NeRFs increases, Rad-NeRF consistently obtains average performance gains on the ScanNet dataset while only marginally increasing the number of model parameters. Compared with directly increasing the hidden dimension of MLP decoders or the size of the feature grid, Rad-NeRF has better performance-model size scalability. Furthermore, we observe that the model with four sub-NeRFs converges faster than the one with two sub-NeRFs while achieving better rendering quality with the same training iterations, as Figure 7 shows. The ease of training convergence can be attributed to two aspects. On the one hand, the number of learnable parameters and training complexity increases marginally. On the other hand, our gate module (a 4-layer MLP without sinusoidal position encoding) decouples the training in the ray dimension and reduces training interference.

5.3 Comparison with Gaussian Splatting

We additionally compare Rad-NeRF against 3D Gaussian splatting (3DGS) [11] as a non-neural approach that represents the current state of the art with regard to quality and rendering speed. The comparison is conducted on MaskTAT [13] and ScanNet [6] datasets. MaskTAT is an object dataset without point clouds, and ScanNet contains indoor scenes with many less textured regions.

Rad-NeRF performs better than 3DGS in some cases. We report results on Table 9, and show qualitative highlights in Figure 8. For the MaskTAT dataset, we initialize 3D GS with random points. Our method performs best over 3D GS and Instant-NGP. For the ScanNet dataset, we initialize 3D GS with the point cloud provided by the dataset. However, there are many less textured regions in

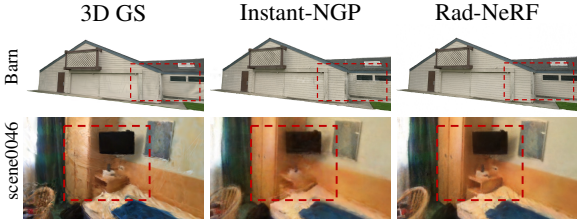

Figure 8: Qualitative comparisons with 3D GS.

Methods	MaskTAT	ScanNet
	PSNR↑	PSNR↑
3D GS	27.363	26.781
Instant-NGP	28.752	28.074
Rad-NeRF	**29.774**	**28.870**

Figure 9: Quantitative results.

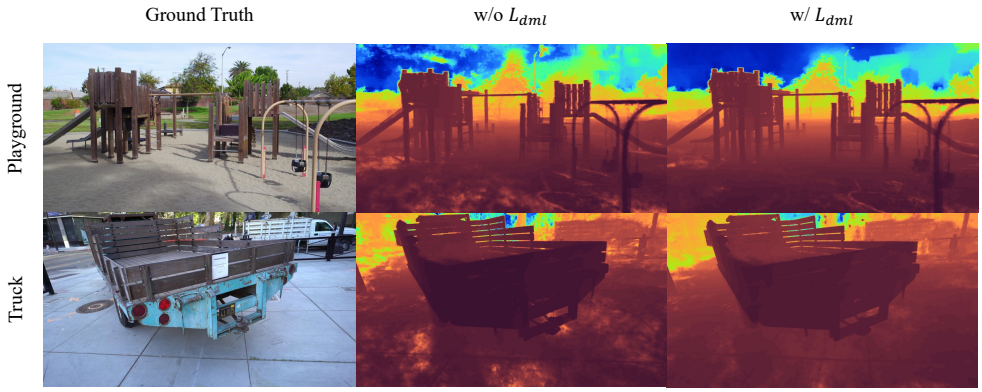

Figure 10: Depth visualization comparison between w/o L_{dml} and w/ L_{dml} on TAT dataset. Zoom in to see the details of sky and ground.

Table 2: Ablation results of gate-guided multi-NeRF fusion and depth-based mutual learning.

Method	Metric	M60	Playground	Train	Truck	Avg
Uniform fusion	PSNR↑	19.229	22.863	17.531	23.569	20.798
	SSIM↑	0.633	0.694	0.596	0.746	0.667
	LPIPS↓	0.431	0.414	0.451	0.345	0.411
w/o depth mutual loss	PSNR↑	18.912	23.399	17.371	24.665	21.087
	SSIM↑	0.621	0.694	0.589	0.758	0.666
	LPIPS↓	0.436	0.402	0.449	0.329	0.404
Rad-NeRF	PSNR↑	19.051	23.901	19.369	24.509	**21.708**
	SSIM↑	0.631	0.689	0.612	0.757	**0.672**
	LPIPS↓	0.429	0.402	0.431	0.333	**0.399**

indoor scenes that affect the accuracy and density of point clouds. Optical distortion exists in the rendered pictures of 3D GS. In contrast, Rad-NeRF renders more smoothly than all baselines.

Potential combination of Rad-NeRF with 3DGS. NeRF is characterized by its neural network-based ray-related predictions, which provide flexibility for cross-scene generalization and enable the application of Rad-NeRF's ray-wise training decoupling approach. In contrast, the plain 3D GS framework parametrizes the scene using a global, non-ray-related representation, making Rad-NeRF inapplicable. However, Rad-NeRF could potentially be applied to generalizable 3D GS frameworks that integrate neural network-based ray-related predictions [4].

5.4 Ablation Studies

In this section, we conduct ablation studies on Rad-NeRF using the TAT dataset [13]. The key takeaways from our results are summarized below. Some additional ablation studies and analyses are presented in the Appendix E.

Importance of the gate-guided multi-NeRF fusion and depth-based mutual learning. The ablation results of the two key components are shown in Table 2. Uniform fusion simply averages multi-NeRFs' outputs to get final results without a gate module. In this way, sub-NeRFs focus on all the training rays instead of having their own preferences, which can not effectively improve rendering quality. For the depth-based mutual learning method, we observe that it enables a smoother and more reasonable depth prediction, as shown in Figure 10. In addition to improving rendering consistency, it also acts as a geometric regularization to reduce the depth ambiguity and avoid overfitting.

We further provide visualizations of different sub-NeRFs' rendering results in Figure 11, which validates that the proposed depth-based mutual learning scheme will not encourage all sub-NeRFs to converge to the same output. On the one hand, the soft gating module allocates different rays to different sub-NeRFs, making them learn from different views. On the other hand, the depth-based mutual learning scheme only lets sub-NeRFs learn the depth from each other rather than the overall rendered density or RGB distribution.

Figure 11: Independent and fused rendering results of sub-NeRFs on TAT dataset.

Table 3: Ablation results of fusion dimensions.

Fusion Dimension	PSNR↑	SSIM↑	LPIPS↓
Point-level	20.796	0.661	0.413
Ray-level (Ours)	**21.708**	**0.672**	**0.399**

Table 4: Ablation results of fusion granularity.

Fusion Granularity	PSNR↑	SSIM↑	LPIPS↓
Image-level	21.503	0.669	0.408
Pixel-level (Ours)	**21.708**	**0.672**	**0.399**

Importance of the ray-level allocation. We evaluate the results of different fusion dimensions in Table 3. Compared to fusing multi-NeRFs' outputs in the point dimension, our ray-based method performs better, validating the superiority of the visibility-aware multi-NeRF method.

Importance of pixel-granularity fusion. We compare different fusion granularity in Table 4. In image-granularity fusion, all pixels of an image have the same preference for model parameters, which may not be reasonable. An illustrative example is an image capturing both the central object and the background region, such as the *Truck* scene shown in Figure 5. In such a case, the rays hitting these two regions should be assigned different model parameters. In contrast, pixel-granularity fusion provides a more fine-grained understanding of the image and scene.

6 Limitations

As the gating module (a 4-layer MLP without sinusoidal position encoding) incorporates smoothness prior implicitly, it exhibits smooth and close scores to the nearest seen view for unseen views. Consequently, the generalization of the gating module relies on sufficient training data, and thus Rad-NeRF does not perform well in the few-shot setting (see Appendix K for more results). On the contrary, the proposed method is suitable for the rendering of complex scenes, which themselves often require sufficient training data.

7 Conclusion

This work proposes a ray-decoupled training framework (Rad-NeRF) for neural rendering. To alleviate the issue of the training interference problem in complex scenes, we construct a multi-NeRF framework and decouple the training of NeRFs in the ray dimension. Additionally, we propose a depth-based mutual learning method that improves the multi-NeRF rendering consistency and reduces the depth ambiguity, thereby improving generalization to novel views. Extensive experiments across various datasets validate Rad-NeRF's effectiveness and better performance-parameter scalability.

We prospect for further exploration to fully exploit the potential of Rad-NeRF. Here, we outline several possible directions:(1) As researchers may choose different frameworks based on specific situational requirements, adapting Rad-NeRF to different single-NeRF frameworks including 3D GS (non-neural approach) is a valuable next step. (2) The number of sub-NeRFs can be determined automatically based on scene complexity and training resources. (3) We hope the newly proposed scaling dimension, which increases the number of sub-NeRFs through ray-wise decoupling, will enable modeling of complex scenes in a parameter-efficient manner.

Acknowledgments

Lidong Guo, Xuefei Ning, Tianchen Zhao, Jincheng Yu, Yu Wang was supported by the National Key R&D Program of China (2023YFB4502200), the National Natural Science Foundation of China (No. 62325405, 62104128, U21B2031, 62204164), Tsinghua EE Xilinx AI Research Fund, Tsinghua-Meituan Joint Institute for Digital Life, and Beijing National Research Center for Information Science and Technology (BNRist).

References

[1] Barron, J.T., Mildenhall, B., Tancik, M., Hedman, P., Martin-Brualla, R., Srinivasan, P.P.: Mip-nerf: A multiscale representation for anti-aliasing neural radiance fields. In: Proceedings of the IEEE/CVF International Conference on Computer Vision. pp. 5855–5864 (2021)

[2] Barron, J.T., Mildenhall, B., Verbin, D., Srinivasan, P.P., Hedman, P.: Mip-nerf 360: Unbounded anti-aliased neural radiance fields. In: Proceedings of the IEEE/CVF Conference on Computer Vision and Pattern Recognition. pp. 5470–5479 (2022)

[3] Barron, J.T., Mildenhall, B., Verbin, D., Srinivasan, P.P., Hedman, P.: Zip-nerf: Anti-aliased grid-based neural radiance fields. arXiv preprint arXiv:2304.06706 (2023)

[4] Charatan, D., Li, S.L., Tagliasacchi, A., Sitzmann, V.: pixelsplat: 3d gaussian splats from image pairs for scalable generalizable 3d reconstruction. In: Proceedings of the IEEE/CVF Conference on Computer Vision and Pattern Recognition. pp. 19457–19467 (2024)

[5] Chen, A., Xu, Z., Geiger, A., Yu, J., Su, H.: Tensorf: Tensorial radiance fields. In: European Conference on Computer Vision. pp. 333–350. Springer (2022)

[6] Dai, A., Chang, A.X., Savva, M., Halber, M., Funkhouser, T., Nießner, M.: Scannet: Richly-annotated 3d reconstructions of indoor scenes. In: Proceedings of the IEEE conference on computer vision and pattern recognition. pp. 5828–5839 (2017)

[7] Deng, K., Liu, A., Zhu, J.Y., Ramanan, D.: Depth-supervised nerf: Fewer views and faster training for free. In: Proceedings of the IEEE/CVF Conference on Computer Vision and Pattern Recognition. pp. 12882–12891 (2022)

[8] Fridovich-Keil, S., Yu, A., Tancik, M., Chen, Q., Recht, B., Kanazawa, A.: Plenoxels: Radiance fields without neural networks. In: Proceedings of the IEEE/CVF Conference on Computer Vision and Pattern Recognition. pp. 5501–5510 (2022)

[9] Goli, L., Reading, C., Sellán, S., Jacobson, A., Tagliasacchi, A.: Bayes' rays: Uncertainty quantification for neural radiance fields. In: Proceedings of the IEEE/CVF Conference on Computer Vision and Pattern Recognition. pp. 20061–20070 (2024)

[10] Jain, A., Tancik, M., Abbeel, P.: Putting nerf on a diet: Semantically consistent few-shot view synthesis. In: Proceedings of the IEEE/CVF International Conference on Computer Vision. pp. 5885–5894 (2021)

[11] Kerbl, B., Kopanas, G., Leimkühler, T., Drettakis, G.: 3d gaussian splatting for real-time radiance field rendering. ACM Transactions on Graphics **42**(4) (2023)

[12] Kim, M., Seo, S., Han, B.: Infonerf: Ray entropy minimization for few-shot neural volume rendering. In: Proceedings of the IEEE/CVF Conference on Computer Vision and Pattern Recognition. pp. 12912–12921 (2022)

[13] Knapitsch, A., Park, J., Zhou, Q.Y., Koltun, V.: Tanks and temples: Benchmarking large-scale scene reconstruction. ACM Transactions on Graphics (ToG) **36**(4), 1–13 (2017)

[14] Liu, S., Zhang, X., Zhang, Z., Zhang, R., Zhu, J.Y., Russell, B.: Editing conditional radiance fields. In: Proceedings of the IEEE/CVF international conference on computer vision. pp. 5773–5783 (2021)

[15] Martin-Brualla, R., Radwan, N., Sajjadi, M.S., Barron, J.T., Dosovitskiy, A., Duckworth, D.: Nerf in the wild: Neural radiance fields for unconstrained photo collections. In: Proceedings of the IEEE/CVF Conference on Computer Vision and Pattern Recognition. pp. 7210–7219 (2021)

[16] Mildenhall, B., Srinivasan, P.P., Ortiz-Cayon, R., Kalantari, N.K., Ramamoorthi, R., Ng, R., Kar, A.: Local light field fusion: Practical view synthesis with prescriptive sampling guidelines. ACM Transactions on Graphics (ToG) **38**(4), 1–14 (2019)

[17] Mildenhall, B., Srinivasan, P.P., Tancik, M., Barron, J.T., Ramamoorthi, R., Ng, R.: Nerf: Representing scenes as neural radiance fields for view synthesis. Communications of the ACM **65**(1), 99–106 (2021)

[18] Müller, T., Evans, A., Schied, C., Keller, A.: Instant neural graphics primitives with a multiresolution hash encoding. ACM Transactions on Graphics (ToG) **41**(4), 1–15 (2022)

[19] Niemeyer, M., Barron, J.T., Mildenhall, B., Sajjadi, M.S., Geiger, A., Radwan, N.: Regnerf: Regularizing neural radiance fields for view synthesis from sparse inputs. In: Proceedings of the IEEE/CVF Conference on Computer Vision and Pattern Recognition. pp. 5480–5490 (2022)

[20] Oechsle, M., Peng, S., Geiger, A.: Unisurf: Unifying neural implicit surfaces and radiance fields for multi-view reconstruction. In: Proceedings of the IEEE/CVF International Conference on Computer Vision. pp. 5589–5599 (2021)

[21] Reiser, C., Peng, S., Liao, Y., Geiger, A.: Kilonerf: Speeding up neural radiance fields with thousands of tiny mlps. In: Proceedings of the IEEE/CVF International Conference on Computer Vision. pp. 14335–14345 (2021)

[22] Sabour, S., Vora, S., Duckworth, D., Krasin, I., Fleet, D.J., Tagliasacchi, A.: Robustnerf: Ignoring distractors with robust losses. In: Proceedings of the IEEE/CVF Conference on Computer Vision and Pattern Recognition. pp. 20626–20636 (2023)

[23] Shazeer, N., Mirhoseini, A., Maziarz, K., Davis, A., Le, Q., Hinton, G., Dean, J.: Outrageously large neural networks: The sparsely-gated mixture-of-experts layer. arXiv preprint arXiv:1701.06538 (2017)

[24] Shazeer, N., Mirhoseini, A., Maziarz, K., Davis, A., Le, Q., Hinton, G., Dean, J.: Outrageously large neural networks: The sparsely-gated mixture-of-experts layer. arXiv preprint arXiv:1701.06538 (2017)

[25] Sun, C., Sun, M., Chen, H.T.: Direct voxel grid optimization: Super-fast convergence for radiance fields reconstruction. In: Proceedings of the IEEE/CVF Conference on Computer Vision and Pattern Recognition. pp. 5459–5469 (2022)

[26] Tancik, M., Casser, V., Yan, X., Pradhan, S., Mildenhall, B., Srinivasan, P.P., Barron, J.T., Kretzschmar, H.: Block-nerf: Scalable large scene neural view synthesis. In: Proceedings of the IEEE/CVF Conference on Computer Vision and Pattern Recognition. pp. 8248–8258 (2022)

[27] Turki, H., Ramanan, D., Satyanarayanan, M.: Mega-nerf: Scalable construction of large-scale nerfs for virtual fly-throughs. In: Proceedings of the IEEE/CVF Conference on Computer Vision and Pattern Recognition. pp. 12922–12931 (2022)

[28] Wang, P., Fan, Z., Chen, T., Wang, Z.: Neural implicit dictionary learning via mixture-of-expert training. In: International Conference on Machine Learning. pp. 22613–22624. PMLR (2022)

[29] Wang, P., Liu, L., Liu, Y., Theobalt, C., Komura, T., Wang, W.: Neus: Learning neural implicit surfaces by volume rendering for multi-view reconstruction. arXiv preprint arXiv:2106.10689 (2021)

[30] Wang, P., Liu, Y., Chen, Z., Liu, L., Liu, Z., Komura, T., Theobalt, C., Wang, W.: F2-nerf: Fast neural radiance field training with free camera trajectories. In: Proceedings of the IEEE/CVF Conference on Computer Vision and Pattern Recognition. pp. 4150–4159 (2023)

[31] Wei, Y., Liu, S., Rao, Y., Zhao, W., Lu, J., Zhou, J.: Nerfingmvs: Guided optimization of neural radiance fields for indoor multi-view stereo. In: Proceedings of the IEEE/CVF International Conference on Computer Vision. pp. 5610–5619 (2021)

[32] Yang, B., Bao, C., Zeng, J., Bao, H., Zhang, Y., Cui, Z., Zhang, G.: Neumesh: Learning disentangled neural mesh-based implicit field for geometry and texture editing. In: European Conference on Computer Vision. pp. 597–614. Springer (2022)

[33] Yang, B., Zhang, Y., Xu, Y., Li, Y., Zhou, H., Bao, H., Zhang, G., Cui, Z.: Learning object-compositional neural radiance field for editable scene rendering. In: Proceedings of the IEEE/CVF International Conference on Computer Vision. pp. 13779–13788 (2021)

[34] Yang, J., Pavone, M., Wang, Y.: Freenerf: Improving few-shot neural rendering with free frequency regularization. In: Proceedings of the IEEE/CVF Conference on Computer Vision and Pattern Recognition. pp. 8254–8263 (2023)

[35] Yariv, L., Gu, J., Kasten, Y., Lipman, Y.: Volume rendering of neural implicit surfaces. Advances in Neural Information Processing Systems **34**, 4805–4815 (2021)

[36] Yu, A., Li, R., Tancik, M., Li, H., Ng, R., Kanazawa, A.: Plenoctrees for real-time rendering of neural radiance fields. In: Proceedings of the IEEE/CVF International Conference on Computer Vision. pp. 5752–5761 (2021)

[37] Zhang, K., Riegler, G., Snavely, N., Koltun, V.: Nerf++: Analyzing and improving neural radiance fields. arXiv preprint arXiv:2010.07492 (2020)

[38] Zhenxing, M., Xu, D.: Switch-nerf: Learning scene decomposition with mixture of experts for large-scale neural radiance fields. In: The Eleventh International Conference on Learning Representations (2022)

Appendix

Table of Contents

A Comparison with Other Multi-NeRF Methods

The comparison of various multi-NeRF training frameworks is summarized in Table S.1. NeRF++ [37] proposes the sphere inversion transformation to map an infinite space to a bounded sphere firstly, and uses two NeRFs to model the 3D points in foreground and background regions, respectively. It adopts the manual allocation mode as it manually sets the boundary between foreground and background regions. Block-NeRF [26] and Mega-NeRF [27] are two classical ray-based multi-NeRF frameworks, which perform the ray allocation in the image-granularity and pixel-granularity, respectively. The former work trains sub-NeRFs in large-scale road scenes with prior knowledge of the image shooting position distribution on the road, and the latter one trains sub-NeRFs in open drone scenes and allocates the rays by partitioning the intersecting positions between the rays and a horizontal plane. However, they are designed for large road scenes and open drone scenes specifically and need a manually defined allocation rule, which requires prior scene knowledge and cannot be easily adapted to other types of scenes. Switch-NeRF [38] implements a learning-based scene partition scheme motivated by Mixture-of-Experts (MoE) [24]. However, it partitions the scene in the point dimension, which limits the rendering performance in more complex scenes with occlusions. It is also limited to be only used in open drone scenes. F2-NeRF [30] is another point-based multi-NeRF method, which allocates the 3D points to multiple sub-NeRFs in a more elaborate but manual way.

In contrast, our Rad-NeRF performs the allocation and decoupling the training in the ray dimension softly. Acting as a ray-based training framework, Rad-NeRF is "visibility-aware" and achieves higher performance in complex scenes. Moreover, compared to other multi-NeRF methods, Rad-NeRF boosts rendering quality across different types of scenes without the need for prior scene knowledge.

Table S.1: Comparison of multi-NeRF training frameworks. **Headers:** The "Dimension" column indicates the dimension in which the framework divides the training data into multiple sub-NeRFs; The "Allocation mode" column indicates whether the framework divides the training data based on the manually designed rule or in a learnable way; The "Target scene" column indicates the scene that the framework is proposed for specifically.

Multi-NeRF methods	Dimension	Allocation mode	Target scene
NeRF++ [37]	point-based	manual	no constraint
Block-NeRF [26]	ray-based	manual	large road scene
Mega-NeRF [27]	ray-based	manual	open drone scene
Switch-NeRF [38]	point-based	learnable	open drone scene
F2-NeRF [30]	point-based	manual	no constraint
Rad-NeRF (ours)	**ray-based**	**learnable**	**no constraint**

B Implementation Details

B.1 Implementation Details of Rad-NeRF

Architecture Details. Our Rad-NeRF is built upon Instant-NGP [18] using a third-party PyTorch implementation [3] and costs no more than one hour of training. We follow the original architecture of Instant-NGP with 16 levels of resolution. The hash table length at each resolution is fixed to 2^{19}. The density and color MLP comprise one and two hidden layers with 64 channels respectively.

Training Details. For Instance-NGP and our Rad-NeRF, we train the NeRFs for 20k iterations on a single RTX-3090 GPU. We use Adam optimizer with a batch size of 8192 rays and a learning rate decaying from 1×10^{-2} to 3×10^{-4}. For the weights of the regularization terms in Equation 6, λ_1 is set to 1×10^{-4} on NeRF-360-v2 and Free dataset, and is set to 5×10^{-3} on other datasets. We set λ_2 to 1×10^{-2} on all the datasets. By default, the number of sub-NeRFs is set to 2, and it is sufficient to achieve significant rendering quality improvement.

Some previous work has observed that the gate module tends to converge to an imbalanced state, where it always produces large weights for the same few sub-models [23, 28, 38]. Such an imbalance

[3] https://github.com/kwea123/ngp_pl

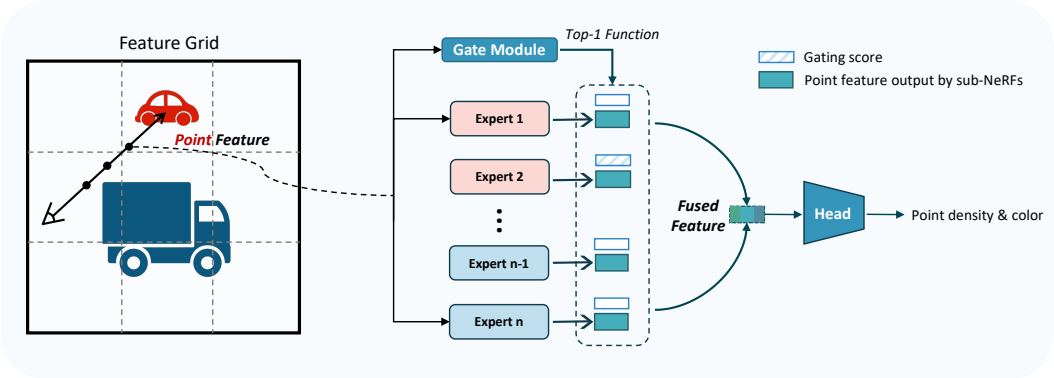

Figure S.1: The overview of Switch-NGP.

problem exists in Rad-NeRF as well. Once the gate module is trapped in a local optimum solution, it will always choose a specific sub-NeRF for rendering and can't effectively decouple the training in the ray dimension.

Following [23, 28], we adopt the regularization on the Coefficient of Variation of the soft gating scores, which encourages a balanced allocation of model parameters for training rays. The CV loss function is given by

$$L_{cv} = \frac{\mathrm{Var}(\overline{G}(\mathcal{R}))}{\left(\sum_{k=1}^{n} \overline{G_k}(\mathcal{R})/n\right)^2}, \tag{7}$$

$$\overline{G_k}(\mathcal{R}) = \sum_{\mathbf{r}\in\mathcal{R}} G_k(\mathbf{r}), \tag{8}$$

where $\overline{G}(\mathcal{R})$ is the set $\left\{\overline{G_k}(\mathcal{R})\right\}_{k=1}^{n}$. Note that some work also uses the load-balanced loss to encourage multi-models to receive roughly equal numbers of training examples [23, 38]. However, this optimization objective is too strict and unsuitable for our framework.

B.2 Implementation Details of Switch-NGP

Switch-NeRF [38] constructs a point-based multi-NeRF framework based on MLP-based NeRF structure. Given a 3D point x, it first extracts high-level point feature $S(x)$ using a linear layer, which will be sent to the gate module to obtain the gating scores. Then, they apply a Top-1 function on the gating scores to determine which NeRF expert should be activated. The output feature of the chosen expert will be multiplied by the gating score corresponding to the expert and obtain the fused point feature. Finally, the fused point feature is sent to the unified MLPs to predict the density σ and color c.

As illustrated in Figure S.1, we build an NGP-version of Switch-NeRF, named Switch-NGP. Since NGP contains a feature grid in the form of the hash table, we directly use the feature grid to obtain the high-level point feature $S(x)$ of the point x. Switch-NeRF has validated the importance of a unified head, wherein the gating score is multiplied by the high-level features rather than the density or color predictions, which makes the gating and prediction more stable in training. We also perform the multi-NeRF fusion in the point-feature dimension by inserting extra K feature MLPs before the density MLP. Each expert in Switch-NGP corresponds to a tiny feature MLP with two hidden layers and 64 channels.

The training details of Switch-NGP are the same as Rad-NeRF, as described in Section B.1.

B.3 Implementation Details of Block-NGP

Block-NeRF [26] applies the multi-NeRF method to the street scene, which allocates model parameters in the ray dimension but in the image-level granularity. Specifically, Block-NeRF places one NeRF at each intersection and directly allocates the training images to multi-NeRFs according to the image shooting positions. We implement an NGP-version Block-NeRF, named Block-NGP, which

can be applied to various types of scenes without prior knowledge. After getting all the training images, we first use the clustering algorithm (KMeans) to cluster the image shooting positions, and the number of clusters is set the same as the number of sub-NeRFs. During the training process, each training image is allocated to the corresponding sub-NeRF according to the clustering results, and the training of sub-NeRFs is independent.

C Experiments on ScanNet Dataset

We compare Rad-NeRF with other multi-NeRF work on ScanNet dataset [6]. Compared to other outdoor datasets, ScanNet contains more texture-less regions like the floors and the walls, which poses more challenges for neural rendering. We conduct experiments in four complete scenes in ScanNet, namely scene0046, scene0276, scene0515 and scene0673. The quantitative and qualitative results are shown in Table S.2 and Figure S.2 respectively. Our Rad-NeRF outperforms other multi-NeRF methods and renders less blur.

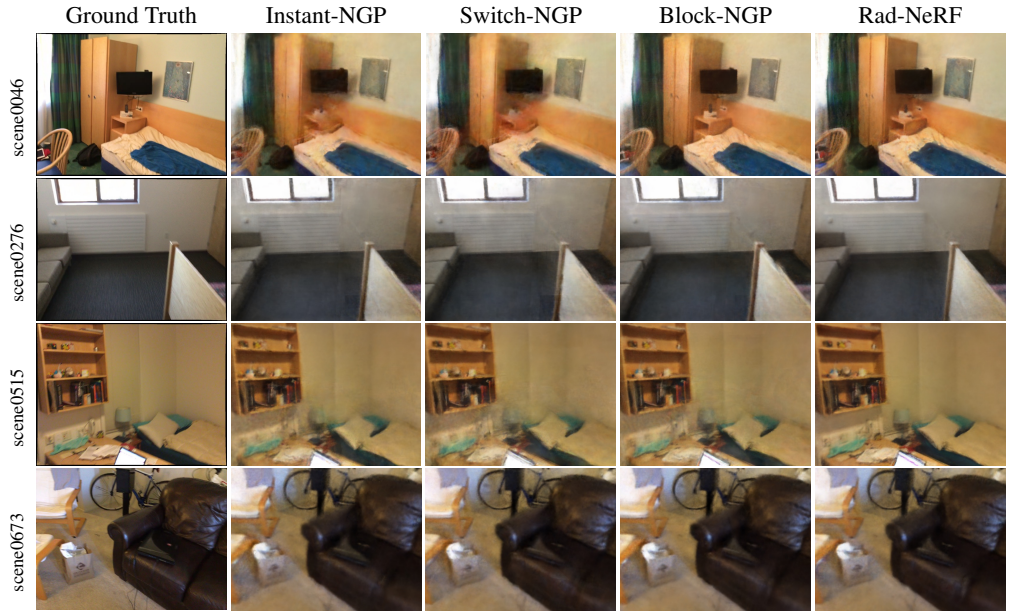

Figure S.2: Qualitative comparisons on ScanNet dataset. Compared to other multi-NeRF methods, Rad-NeRF renders less blur and achieves better recovery of details.

Table S.2: Quantitative results on ScanNet dataset.

Methods	Metrics	scene0046	scene0276	scene0515	scene0673	Avg
NGP	PSNR↑	28.504	29.996	28.159	25.278	27.984
	SSIM↑	0.839	0.835	0.786	0.686	0.786
	LPIPS↓	0.413	0.421	0.448	0.472	0.438
Switch-NGP	PSNR↑	28.135	29.614	27.814	25.140	27.676
	SSIM↑	0.834	0.831	0.779	0.684	0.782
	LPIPS↓	0.421	0.431	0.456	0.473	0.445
Block-NGP	PSNR↑	28.728	30.214	28.332	25.444	28.180
	SSIM↑	0.842	0.840	0.789	0.688	0.790
	LPIPS↓	0.408	0.416	0.443	0.469	0.434
Rad-NeRF	PSNR↑	29.440	30.871	29.149	25.759	**28.805**
	SSIM↑	0.851	0.843	0.800	0.690	**0.796**
	LPIPS↓	0.396	0.405	0.427	0.469	**0.424**

D Per-Scene Results

We provide the per-scene quantitative results on the Mask-TAT dataset, TAT dataset, NeRF-360-v2 dataset and Free dataset in Table S.3, Table S.4, Table S.5 and Table S.6 respectively. The results are reported in the metric of PSNR.

Table S.3: Scene breakdown on the Mask-TAT dataset.

Methods	Ignatius	Truck	Barn	Caterpillar	Family	Avg
NeRF	25.43	25.36	24.05	23.75	30.29	25.78
MipNeRF	29.037	23.19	28.481	28.016	29.009	27.547
PlenOctrees	28.19	26.83	26.8	25.29	32.85	27.99
DVGO	28.16	27.15	27.01	26.00	33.75	28.41
Instant-NGP	28.431	27.562	27.611	26.065	34.092	28.752
Switch-NGP	28.184	27.34	27.472	25.75	33.711	28.491
Block-NGP	28.202	27.621	27.768	26.06	34.081	28.746
Rad-NeRF	29.806	28.163	28.701	27.445	34.756	29.774

Table S.4: Scene breakdown on the TAT dataset.

Methods	M60	Playground	Train	Truck	Avg
NeRF	16.86	21.55	16.64	20.85	18.975
NeRF++	17.964	22.914	18.194	22.603	20.419
MipNeRF-360	20.091	24.27	19.741	24.144	22.062
MipNeRF360$_{short}$	18.394	22.682	17.738	21.497	20.078
DVGO	17.292	22.62	17.783	21.306	19.750
Instant-NGP	18.914	22.832	17.707	23.428	20.720
Switch-NGP	18.619	22.661	17.523	23.243	20.512
Block-NGP	18.879	22.555	18.048	23.651	20.783
Rad-NeRF	19.051	23.901	19.369	24.509	21.708

Table S.5: Scene breakdown on the NeRF-360-v2 dataset.

Methods	bicycle	bonsai	counter	garden	kitchen	room	stump	Avg
NeRF	21.818	29.028	26.980	23.640	27.164	30.097	22.934	25.952
NeRF++	21.426	31.670	27.717	24.801	29.468	30.621	24.770	27.210
MipNeRF360	22.861	32.970	29.291	26.014	31.987	32.685	25.278	28.727
MipNeRF360$_{short}$	21.264	28.040	26.366	23.214	26.552	29.636	23.313	25.484
DVGO	21.652	27.919	26.432	23.851	26.282	31.677	20.988	25.543
F2-NeRF	21.311	30.036	25.873	23.694	28.935	29.421	24.251	26.217
Instant-NGP	24.203	31.374	25.665	25.312	30.278	31.534	22.799	27.309
Switch-NGP	23.859	30.012	24.359	25.164	29.865	31.127	21.284	26.524
Block-NGP	24.186	31.684	25.704	25.288	30.382	31.569	23.241	27.436
Rad-NeRF	24.550	32.439	25.230	25.634	31.062	32.863	23.312	27.871

E Additional Ablation Studies

We add additional ablation studies on the TAT dataset to further analyze the mechanism of Rad-NeRF, including structural design, depth-mutual learning, and CV-balanced regularization. The results are shown in Table S.7.

Gate-guided depth mutual learning. In Rad-NeRF, we use the gate-guided fused depth as the target depth to regularize sub-NeRFs' geometry and avoid overfitting. By contrast, when we directly use

Table S.6: Scene breakdown on the Free dataset

Methods	Hydrant	Lab	Pillar	Road	Sky	Stair	Grass	Avg
NeRF	16.569	17.342	20.944	19.793	15.925	18.731	22.439	18.820
NeRF++	22.948	23.718	26.353	24.916	25.059	27.647	21.504	24.592
MipNeRF360	25.03	26.57	29.22	27.07	26.99	29.79	24.39	27.008
MipNeRF360$_{short}$	23.281	24.412	26.789	24.158	25.369	27.139	21.827	24.711
DVGO	22.315	23.123	25.345	23.242	24.736	25.844	19.794	23.485
Instant-NGP	23.29	26.084	28.683	26.302	26.05	28.158	23.088	25.951
F2-NeRF	24.34	25.92	28.76	26.76	26.41	29.19	22.87	26.32
Switch-NGP	23.197	25.901	28.080	26.155	26.034	28.097	22.819	25.755
Block-NGP	23.663	26.682	28.103	25.989	26.283	28.395	22.988	26.015
Rad-NeRF	24.463	25.751	28.871	26.827	27.235	28.562	23.433	26.449

the average of the sub-NeRFs' rendering depths as the target depth, which means all sub-NeRFs have equal regularization strength (Equal DML), the rendering quality will be slightly worse. The results highlight the pivotal role of gate-guided depth mutual learning. Using the gated-guided fused depth as the target depth differently penalizes sub-depths based on the gating scores and increases the accuracy of the geometry regularization. We also observe that depth mutual learning has no effect in the case of uniform fusion due to the low accuracy of the averaged depth.

CV balanced regularization. As introduced in Section B.1, we adopt the regularization on the Coefficient of Variation of the soft gating scores to prevent the gate module from collapsing onto a specific sub-NeRF while maintaining sub-NeRF's different specialties. Without CV-balanced regularization, the rendering quality degrades significantly. Besides, we apply the CV regularization only for the first half of the training time and find that the performance is comparable to Rad-NeRF, The results prove that such regularization would not interfere with the learning of the gate module.

Table S.7: Additional ablation results.

Method	Metric	M60	Playground	Train	Truck	Avg
Equal DML	PSNR↑	18.929	23.108	19.012	24.625	21.419
	SSIM↑	0.625	0.686	0.610	0.758	0.670
	LPIPS↓	0.431	0.405	0.432	0.332	0.400
Independent feature grids	PSNR↑	18.765	22.839	18.958	24.493	21.264
	SSIM↑	0.625	0.697	0.614	0.762	0.675
	LPIPS↓	0.431	0.405	0.417	0.325	0.395
Uniform fusion w/o DML	PSNR↑	19.229	22.863	17.531	23.569	20.798
	SSIM↑	0.633	0.694	0.596	0.746	0.667
	LPIPS↓	0.431	0.414	0.451	0.345	0.411
Uniform fusion w/ DML	PSNR↑	19.005	22.766	17.532	23.513	20.704
	SSIM↑	0.627	0.695	0.592	0.747	0.665
	LPIPS↓	0.434	0.411	0.453	0.341	0.410
w/o CV loss	PSNR↑	18.743	22.795	17.245	23.395	20.545
	SSIM↑	0.619	0.683	0.587	0.731	0.655
	LPIPS↓	0.445	0.419	0.465	0.354	0.421
Half CV loss	PSNR↑	19.114	24.003	19.462	24.518	21.774
	SSIM↑	0.625	0.689	0.606	0.758	0.670
	LPIPS↓	0.433	0.404	0.430	0.334	0.400
Rad-NeRF	PSNR↑	19.051	23.901	19.369	24.509	21.708
	SSIM↑	0.631	0.689	0.612	0.757	0.672
	LPIPS↓	0.429	0.402	0.431	0.333	0.399

Structural design. In Rad-NeRF, we adopt a multi-NeRF structure with a shared feature grid and an ensemble of MLP decoders. We further analyze the reason behind the performance improvement and explore the performance of independent feature grids. As Table S.7 shows, the model employing a shared feature grid (Rad-NeRF) outperforms its counterpart with multiple independent feature grids, which highlights the effect of independent MLP decoders rather than feature grids. We attribute this observation and the performance gained by Rad-NeRF to two aspects. (1)Within the hybrid representation, the feature grid is responsible for encoding features of 3D spatial points, while the MLP encoder is designed to encode view information. The crucial design of independent MLP decoders aligns with our visibility-aware motivation, thereby enhancing the view-dependent effect. (2)The training complexity will also increase as the trainable parameters increase. With the limited amount of training data, increasing the number of feature grids leads to poor convergence. By contrast, as different rays may pass through the same region of 3D space, weight sharing for the feature grid helps to facilitate training. Although the number of learnable parameters hardly increases, Rad-NeRF decouples the training in the ray dimension, helping to increase the model's generalization ability.

F Discussion of Mega-NGP

Mega-NeRF [27] applies the multi-NeRF method to the drone scenes, allocating model parameters in the ray dimension and the pixel-level granularity. Specifically, it allocates rays by partitioning the intersecting points between rays and scenes. Such a method is suitable for drone scenes, where the top-down perspective allows for the approximation of ray-scene intersections by intersecting with a set horizontal plane. However, in unstructured scenes captured by free trajectories, the intersecting points between rays and scenes cannot be determined before the training is completed, limiting the applicability of Mega-NeRF to such scenes.

Since there is no straightforward implementation to determine the ray intersections before training, we adopt an alternative implementation for NGP-version Mega-NeRF, which employs a clustering algorithm to divide rays directly based on their origins and directions. The clustering process is offline and the same as the one in Block-NGP. During the training process, each training pixel is allocated to one corresponding sub-NeRF according to the clustering results. To ensure a fair comparison, the model structure of Mega-NGP is the same as the one in Rad-NeRF, following the implementation of Block-NGP. We conduct a comprehensive evaluation across all datasets and the experimental results are shown in Table S.8. Mega-NGP yields similar results to Block-NGP, which is less effective than our Rad-NeRF.

Table S.8: Comparison with Mega-NGP and Rad-NeRF

Method	Metric	TAT	360v2	Free Dataset	ScanNet
Mega-NGP	PSNR↑	20.843	27.482	25.855	28.100
	SSIM↑	0.659	0.761	0.696	0.786
	LPIPS↓	0.415	0.311	0.332	0.437
Rad-NeRF	PSNR↑	21.708	27.87	26.449	28.870
	SSIM↑	0.672	0.769	0.719	0.797
	LPIPS↓	0.399	0.298	0.285	0.424

G More Scalability Studies

We provide the per-scene results of scalability studies on the ScanNet dataset in Table S.9 which are reported in the metric of PSNR.

Furthermore, we observe that the model with four sub-NeRFs converges faster than the one with two sub-NeRFs while achieving better rendering quality with the same training iterations, as Figure S.3 shows. The ease of training convergence can be attributed to two aspects. On the one hand, the feature grid is shared among multi-NeRFs, and thus, the number of learnable parameters increases marginally. On the other hand, as the neural network is better at fitting low-frequency information, our gate module (a 4-layer MLP without sinusoidal position encoding) has implicitly incorporated "smoothness prior", leading to closer rays to be more possibly assigned closer gating scores.

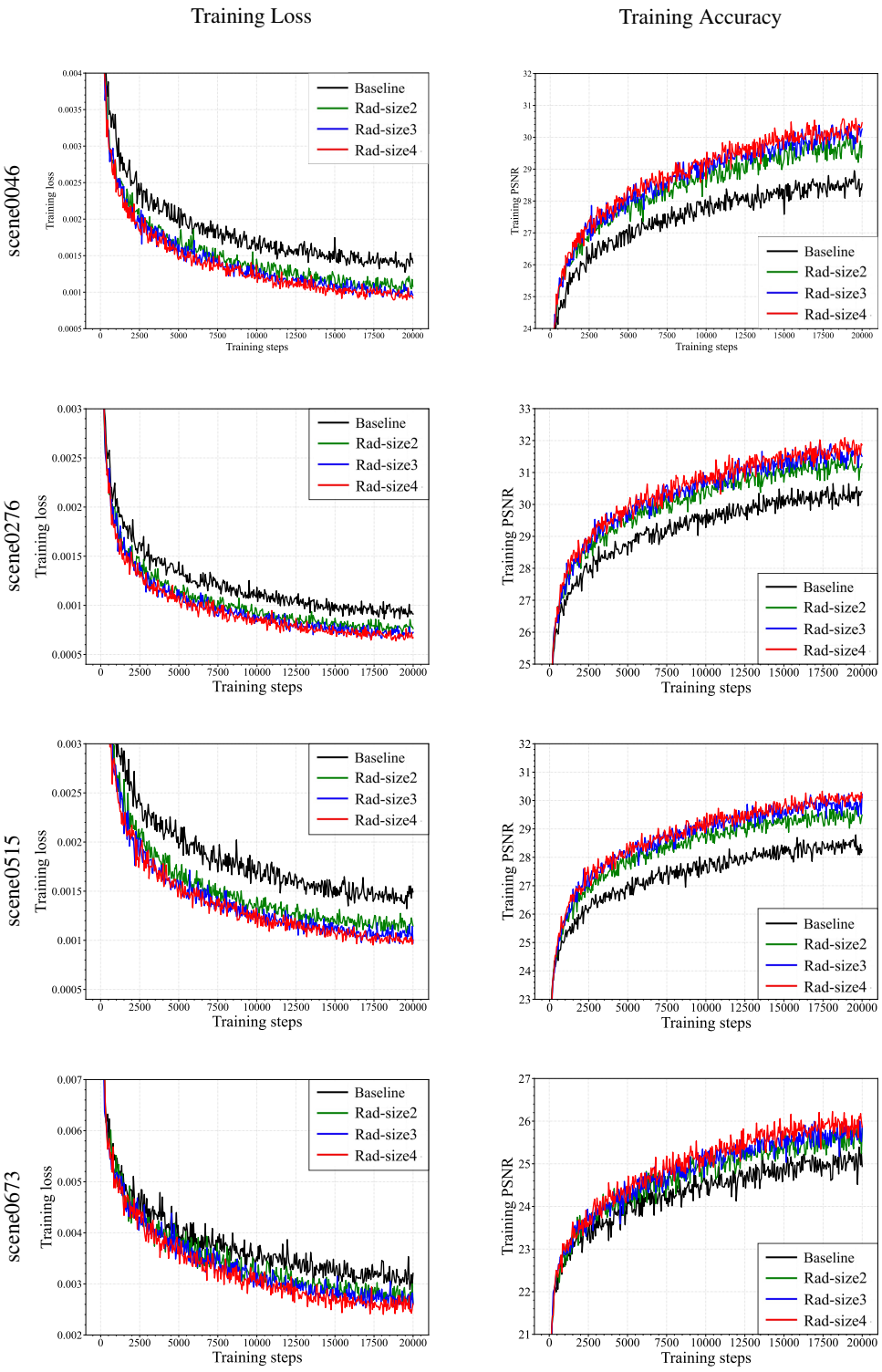

Figure S.3: Convergence curve on the ScanNet dataset.

Table S.9: Scene breakdown of scalability studies on the ScanNet dataset.

Method	004600	027600	051500	067304	Avg
Instant-NGP	28.504	29.996	28.159	25.278	27.984
Rad-NeRF-size2	29.440	30.871	29.149	25.759	28.805
Rad-NeRF-size3	29.878	31.242	29.470	25.944	29.134
Rad-NeRF-size4	30.018	31.310	29.679	26.063	29.268

H The Training and Inference Efficiency of Rad-NeRF

We expand the scalability study in the main paper and supplement additional results about training time and inference speed. The comparison results are shown in Figure S.4. Compared to the Instant-NGP baseline, all methods for scaling up NeRF's capacity require longer training time and exhibit lower inference speed, including scaling the MLP width and different multi-NeRF frameworks. Among these methods, Rad-NeRF achieves the best tradeoff between training/inference efficiency and rendering quality. Since we adopt a shared feature grid and multiple independent MLP decoders in the Rad-NeRF framework, a point feature needs to be processed by MLPs in turn, which is the major cause of reduced efficiency. However, as multiple independent MLP decoders can be combined into a single MLP through appropriate parameter initialization and freezing, Rad-NeRF can obtain further efficiency improvements and approach the efficiency of scaling the MLP width.

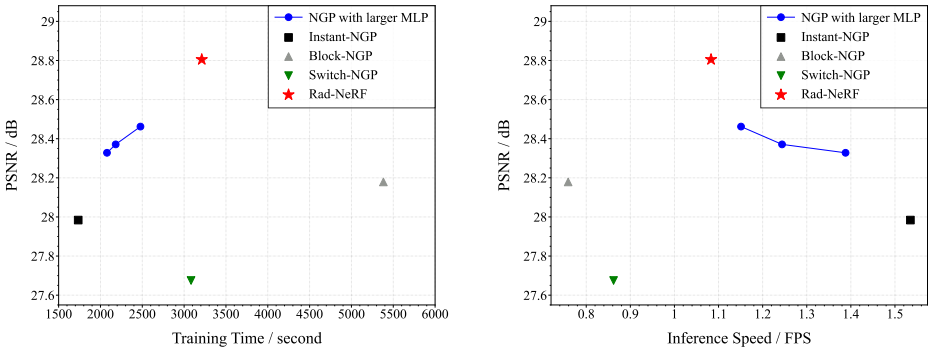

Figure S.4: Scalability study about training/inference efficiency.

I Integration of Rad-NeRF and Zip-NeRF

As a multi-NeRF training framework, Rad-NeRF is essentially orthogonal to the structure and training method of single-NeRF. For the benefit of training efficiency and its wide application, we build and validate Rad-NeRF upon the Instant-NGP. Nevertheless, it can also be integrated with other single-NeRF frameworks, such as ZipNeRF [3] (a SOTA single-NeRF framework).

We implement a ZipNeRF version of Rad-NeRF, named Rad-ZipNeRF, and evaluate the performance on the 360v2 dataset. Similar to Rad-NeRF, Rad-ZipNeRF adopts a shared feature grid and multiple MLP decoders. The training settings are kept the same as the original paper, including the training iterations and batch size. As shown in Table S.10, integrated with Rad-NeRF, ZipNeRF can also obtain performance gains, validating Rad-NeRF's effectiveness and potential for integration with different frameworks.

Considering that different frameworks have different characteristics, researchers may choose different frameworks based on specific situational requirements. Adapting Rad-NeRF to different single-NeRF frameworks remains an interesting point to be explored in the future.

We further validate the performance of Rad-NeRF on the Free dataset [34]. As the results show, Rad-NeRF's multi-NeRF training framework boosts ZipNeRF's performance consistently.

Table S.10: Comparison with ZipNeRF and Rad-ZipNeRF on the 360v2 dataset.

Methods	bicycle	bonsai	counter	garden	kitchen	room	stump	Avg
ZipNeRF	21.019	33.052	25.982	24.330	32.843	34.777	25.406	28.201
Rad-ZipNeRF	20.488	33.486	26.372	24.603	33.120	35.795	25.581	28.492

Table S.11: Comparison with ZipNeRF and Rad-ZipNeRF on the free dataset.

Method	Hydrant	Lab	Pillar	Road	Sky	Stair	Grass	Avg
ZipNeRF	25.402	27.827	25.132	28.882	26.993	28.187	18.461	25.841
Rad-ZipNeRF	25.51	28.067	25.348	29.191	27.491	28.339	18.572	26.074

J Additional Visualizations of Gating Scores

In the visualization results of the main paper, we adopt two sub-NeRFs in all scenes of the TAT dataset. With this setting, the two sub-NeRFs exhibit complementary gating scores for the same view and we omitted the visualization of sub-NeRF2 for brevity in the main paper. We also provide the visualization results of the other sub-NeRF in Figure S.5. As shown in Figure S.5, when rendering in an open scene with fewer occlusions, the gating score exhibits different characteristic and smooth transition according to the ray directions. This visualization further validates our analysis that as a 4-layer MLP without sinusoidal position encoding, the gating module incorporates smoothness prior implicitly. For unseen viewpoints, especially in less-occluded outdoor scenes, the gating module exhibits smooth and close scores to the nearest seen view. The additional visualization results further prove that our original motivation for tackling heavy occlusion by decoupling sub-NeRF training is valid.

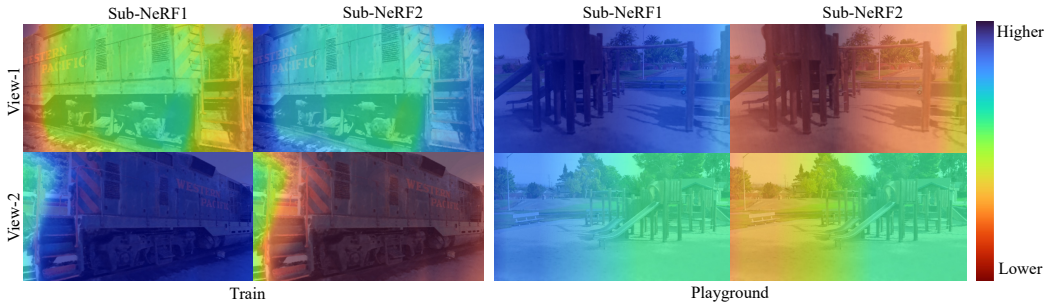

Figure S.5: Additional visualizations of gating scores on two different views on TAT dataset.

K Limitation under the Few-shot Setting

Previously, we have included the discussion of the limitation under the few-shot setting. This is because rendering under the few-shot setting presents a greater challenge to both NeRF's and gating module's generalization ability.

We validate Rad-NeRF's performance in the few-shot setting on the LLFF dataset [16]. For 6/9 training views, Rad-NeRF does not exhibit significant benefits or performance improvements compared to Instant-NGP, with all metrics at the same level. This is because insufficient training data affects the training and generalization of the gating module.

However, when rendering with extremely few training data (3 views), Rad-NeRF achieves significantly better rendering quality. We analyze that when training with very few views, the gating module has minimal impact on NeRF's training. Nonetheless, depth-based mutual learning between multiple sub-NeRFs could still exhibit an effective geometric regularization effect, thereby improving rendering performance. This analysis is also validated by the visualization results shown in Figure S.6, compared to the baseline, Rad-NeRF reduces the depth rendering ambiguity and shows better geometry modeling in a 3-view setting.

Table S.12: Rad-NeRF's performance under the few-shot setting

Method	PSNR↑			SSIM↑			LPIPS↓		
	3-view	6-view	9-view	3-view	6-view	9-view	3-view	6-view	9-view
Instant-NGP	16.107	19.594	21.105	0.419	0.592	0.663	0.541	0.394	0.353
Rad-NeRF	16.626	19.214	20.979	0.452	0.592	0.661	0.506	0.298	0.344

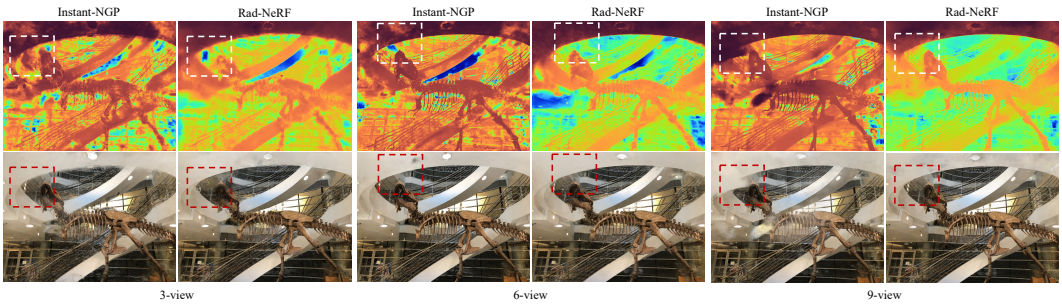

Figure S.6: Qualitative comparisons under three few-shot settings on LLFF dataset.

L Comparison of Rad-NeRF with Uncertainty-based Methods

Uncertainty-based methods consider floaters as regions corresponding to high uncertainty and remove them by thresholding the scene according to an uncertainty field during rendering. The spatial uncertainty is computed in roughly a minute on any existing method. For example, RobustNeRF [22] treated pixels with larger losses as those with high uncertainty, avoiding the misleading effect of outlier points by discarding the training of those pixels. However, it is difficult to distinguish outlier points from the high-frequency areas that should be learned. Moreover, Instant-NGP [18] regards the spatial points with too low density as regions with high uncertainty and filters these regions when rendering. Although this method works well, it still cannot completely eliminate floaters in difficult scenes and may remove correct regions. As a post-hoc uncertainty assessment framework, Bayes Rays [9] acts as a post-hoc uncertainty assessment framework, which does not change NeRF's training process, only removing "floater" regions corresponding to high uncertainty. However, this solution is not stable and is generally used as an auxiliary solution to improve NeRF's rendering quality.

Different from uncertainty-based methods, the proposed Rad-NeRF improves rendering quality by tackling the training interference issue. The depth-based mutual learning method also acts as a geometric regularization to reduce rendering defects. Importantly, Rad-NeRF is essentially orthogonal to these post-training uncertainty removal-based methods and can be integrated with Bayes Rays to obtain further performance improvement.

NeurIPS Paper Checklist

1. **Claims**

   Question: Do the main claims made in the abstract and introduction accurately reflect the paper's contributions and scope?

   Answer: [Yes]

   Justification: We state the intuition and corresponding validation experiments in the introduction section 1. The contribution of ray-decoupled training framework is demonstrated clearly.

   Guidelines:

   - The answer NA means that the abstract and introduction do not include the claims made in the paper.
   - The abstract and/or introduction should clearly state the claims made, including the contributions made in the paper and important assumptions and limitations. A No or NA answer to this question will not be perceived well by the reviewers.
   - The claims made should match theoretical and experimental results, and reflect how much the results can be expected to generalize to other settings.
   - It is fine to include aspirational goals as motivation as long as it is clear that these goals are not attained by the paper.

2. **Limitations**

   Question: Does the paper discuss the limitations of the work performed by the authors?

   Answer: [Yes]

   Justification: We create a separate "Limitations" section 6 in the main paper. We point out the limitation of the proposed Rad-NeRF in the few-shot setting.

   Guidelines:

   - The answer NA means that the paper has no limitation while the answer No means that the paper has limitations, but those are not discussed in the paper.
   - The authors are encouraged to create a separate "Limitations" section in their paper.
   - The paper should point out any strong assumptions and how robust the results are to violations of these assumptions (e.g., independence assumptions, noiseless settings, model well-specification, asymptotic approximations only holding locally). The authors should reflect on how these assumptions might be violated in practice and what the implications would be.
   - The authors should reflect on the scope of the claims made, e.g., if the approach was only tested on a few datasets or with a few runs. In general, empirical results often depend on implicit assumptions, which should be articulated.
   - The authors should reflect on the factors that influence the performance of the approach. For example, a facial recognition algorithm may perform poorly when image resolution is low or images are taken in low lighting. Or a speech-to-text system might not be used reliably to provide closed captions for online lectures because it fails to handle technical jargon.
   - The authors should discuss the computational efficiency of the proposed algorithms and how they scale with dataset size.
   - If applicable, the authors should discuss possible limitations of their approach to address problems of privacy and fairness.
   - While the authors might fear that complete honesty about limitations might be used by reviewers as grounds for rejection, a worse outcome might be that reviewers discover limitations that aren't acknowledged in the paper. The authors should use their best judgment and recognize that individual actions in favor of transparency play an important role in developing norms that preserve the integrity of the community. Reviewers will be specifically instructed to not penalize honesty concerning limitations.

3. **Theory Assumptions and Proofs**

   Question: For each theoretical result, does the paper provide the full set of assumptions and a complete (and correct) proof?

Answer: [NA]

Justification: The paper does not include theoretical results.

Guidelines:

- The answer NA means that the paper does not include theoretical results.
- All the theorems, formulas, and proofs in the paper should be numbered and cross-referenced.
- All assumptions should be clearly stated or referenced in the statement of any theorems.
- The proofs can either appear in the main paper or the supplemental material, but if they appear in the supplemental material, the authors are encouraged to provide a short proof sketch to provide intuition.
- Inversely, any informal proof provided in the core of the paper should be complemented by formal proofs provided in appendix or supplemental material.
- Theorems and Lemmas that the proof relies upon should be properly referenced.

4. **Experimental Result Reproducibility**

   Question: Does the paper fully disclose all the information needed to reproduce the main experimental results of the paper to the extent that it affects the main claims and/or conclusions of the paper (regardless of whether the code and data are provided or not)?

   Answer: [Yes]

   Justification: We have provided all the needed information (e.g.,training settings, hypermeters, and so on) in the Appendix B, ensuring the reproducibility of Rad-NeRF.

   Guidelines:

   - The answer NA means that the paper does not include experiments.
   - If the paper includes experiments, a No answer to this question will not be perceived well by the reviewers: Making the paper reproducible is important, regardless of whether the code and data are provided or not.
   - If the contribution is a dataset and/or model, the authors should describe the steps taken to make their results reproducible or verifiable.
   - Depending on the contribution, reproducibility can be accomplished in various ways. For example, if the contribution is a novel architecture, describing the architecture fully might suffice, or if the contribution is a specific model and empirical evaluation, it may be necessary to either make it possible for others to replicate the model with the same dataset, or provide access to the model. In general. releasing code and data is often one good way to accomplish this, but reproducibility can also be provided via detailed instructions for how to replicate the results, access to a hosted model (e.g., in the case of a large language model), releasing of a model checkpoint, or other means that are appropriate to the research performed.
   - While NeurIPS does not require releasing code, the conference does require all submissions to provide some reasonable avenue for reproducibility, which may depend on the nature of the contribution. For example
     (a) If the contribution is primarily a new algorithm, the paper should make it clear how to reproduce that algorithm.
     (b) If the contribution is primarily a new model architecture, the paper should describe the architecture clearly and fully.
     (c) If the contribution is a new model (e.g., a large language model), then there should either be a way to access this model for reproducing the results or a way to reproduce the model (e.g., with an open-source dataset or instructions for how to construct the dataset).
     (d) We recognize that reproducibility may be tricky in some cases, in which case authors are welcome to describe the particular way they provide for reproducibility. In the case of closed-source models, it may be that access to the model is limited in some way (e.g., to registered users), but it should be possible for other researchers to have some path to reproducing or verifying the results.

5. **Open access to data and code**

Question: Does the paper provide open access to the data and code, with sufficient instructions to faithfully reproduce the main experimental results, as described in supplemental material?

Answer: [Yes]

Justification: We provide all the code in the supplementary material, with detailed instructions and execution scripts.

Guidelines:

- The answer NA means that paper does not include experiments requiring code.
- Please see the NeurIPS code and data submission guidelines (`https://nips.cc/public/guides/CodeSubmissionPolicy`) for more details.
- While we encourage the release of code and data, we understand that this might not be possible, so "No" is an acceptable answer. Papers cannot be rejected simply for not including code, unless this is central to the contribution (e.g., for a new open-source benchmark).
- The instructions should contain the exact command and environment needed to run to reproduce the results. See the NeurIPS code and data submission guidelines (`https://nips.cc/public/guides/CodeSubmissionPolicy`) for more details.
- The authors should provide instructions on data access and preparation, including how to access the raw data, preprocessed data, intermediate data, and generated data, etc.
- The authors should provide scripts to reproduce all experimental results for the new proposed method and baselines. If only a subset of experiments are reproducible, they should state which ones are omitted from the script and why.
- At submission time, to preserve anonymity, the authors should release anonymized versions (if applicable).
- Providing as much information as possible in supplemental material (appended to the paper) is recommended, but including URLs to data and code is permitted.

6. **Experimental Setting/Details**

   Question: Does the paper specify all the training and test details (e.g., data splits, hyperparameters, how they were chosen, type of optimizer, etc.) necessary to understand the results?

   Answer: [Yes]

   Justification: All the necessary experimental details are stated in the Appendix B.

   Guidelines:

   - The answer NA means that the paper does not include experiments.
   - The experimental setting should be presented in the core of the paper to a level of detail that is necessary to appreciate the results and make sense of them.
   - The full details can be provided either with the code, in appendix, or as supplemental material.

7. **Experiment Statistical Significance**

   Question: Does the paper report error bars suitably and correctly defined or other appropriate information about the statistical significance of the experiments?

   Answer: [No]

   Justification: Considering the negligible deviation of NeRF rendering results, we do not report error bars in the quantitative results.

   Guidelines:

   - The answer NA means that the paper does not include experiments.
   - The authors should answer "Yes" if the results are accompanied by error bars, confidence intervals, or statistical significance tests, at least for the experiments that support the main claims of the paper.
   - The factors of variability that the error bars are capturing should be clearly stated (for example, train/test split, initialization, random drawing of some parameter, or overall run with given experimental conditions).

- The method for calculating the error bars should be explained (closed form formula, call to a library function, bootstrap, etc.)
- The assumptions made should be given (e.g., Normally distributed errors).
- It should be clear whether the error bar is the standard deviation or the standard error of the mean.
- It is OK to report 1-sigma error bars, but one should state it. The authors should preferably report a 2-sigma error bar than state that they have a 96% CI, if the hypothesis of Normality of errors is not verified.
- For asymmetric distributions, the authors should be careful not to show in tables or figures symmetric error bars that would yield results that are out of range (e.g. negative error rates).
- If error bars are reported in tables or plots, The authors should explain in the text how they were calculated and reference the corresponding figures or tables in the text.

8. **Experiments Compute Resources**

   Question: For each experiment, does the paper provide sufficient information on the computer resources (type of compute workers, memory, time of execution) needed to reproduce the experiments?

   Answer: [Yes]

   Justification: We indicate the type of GPU and the time of execution (no more than one hour of training) in the Appendix B.

   Guidelines:

   - The answer NA means that the paper does not include experiments.
   - The paper should indicate the type of compute workers CPU or GPU, internal cluster, or cloud provider, including relevant memory and storage.
   - The paper should provide the amount of compute required for each of the individual experimental runs as well as estimate the total compute.
   - The paper should disclose whether the full research project required more compute than the experiments reported in the paper (e.g., preliminary or failed experiments that didn't make it into the paper).

9. **Code Of Ethics**

   Question: Does the research conducted in the paper conform, in every respect, with the NeurIPS Code of Ethics `https://neurips.cc/public/EthicsGuidelines`?

   Answer: [Yes]

   Justification: We have reviewed the NeurIPS Code of Ethics.

   Guidelines:

   - The answer NA means that the authors have not reviewed the NeurIPS Code of Ethics.
   - If the authors answer No, they should explain the special circumstances that require a deviation from the Code of Ethics.
   - The authors should make sure to preserve anonymity (e.g., if there is a special consideration due to laws or regulations in their jurisdiction).

10. **Broader Impacts**

    Question: Does the paper discuss both potential positive societal impacts and negative societal impacts of the work performed?

    Answer: [NA]

    Justification: This paper has no societal impact, since NeRF renders the real scene without any fake generation.

    Guidelines:

    - The answer NA means that there is no societal impact of the work performed.
    - If the authors answer NA or No, they should explain why their work has no societal impact or why the paper does not address societal impact.

- Examples of negative societal impacts include potential malicious or unintended uses (e.g., disinformation, generating fake profiles, surveillance), fairness considerations (e.g., deployment of technologies that could make decisions that unfairly impact specific groups), privacy considerations, and security considerations.
- The conference expects that many papers will be foundational research and not tied to particular applications, let alone deployments. However, if there is a direct path to any negative applications, the authors should point it out. For example, it is legitimate to point out that an improvement in the quality of generative models could be used to generate deepfakes for disinformation. On the other hand, it is not needed to point out that a generic algorithm for optimizing neural networks could enable people to train models that generate Deepfakes faster.
- The authors should consider possible harms that could arise when the technology is being used as intended and functioning correctly, harms that could arise when the technology is being used as intended but gives incorrect results, and harms following from (intentional or unintentional) misuse of the technology.
- If there are negative societal impacts, the authors could also discuss possible mitigation strategies (e.g., gated release of models, providing defenses in addition to attacks, mechanisms for monitoring misuse, mechanisms to monitor how a system learns from feedback over time, improving the efficiency and accessibility of ML).

11. **Safeguards**

    Question: Does the paper describe safeguards that have been put in place for responsible release of data or models that have a high risk for misuse (e.g., pretrained language models, image generators, or scraped datasets)?

    Answer: [NA]

    Justification: This paper poses no such risks.

    Guidelines:

    - The answer NA means that the paper poses no such risks.
    - Released models that have a high risk for misuse or dual-use should be released with necessary safeguards to allow for controlled use of the model, for example by requiring that users adhere to usage guidelines or restrictions to access the model or implementing safety filters.
    - Datasets that have been scraped from the Internet could pose safety risks. The authors should describe how they avoided releasing unsafe images.
    - We recognize that providing effective safeguards is challenging, and many papers do not require this, but we encourage authors to take this into account and make a best faith effort.

12. **Licenses for existing assets**

    Question: Are the creators or original owners of assets (e.g., code, data, models), used in the paper, properly credited and are the license and terms of use explicitly mentioned and properly respected?

    Answer: [NA]

    Justification: This paper does not use existing assets.

    Guidelines:

    - The answer NA means that the paper does not use existing assets.
    - The authors should cite the original paper that produced the code package or dataset.
    - The authors should state which version of the asset is used and, if possible, include a URL.
    - The name of the license (e.g., CC-BY 4.0) should be included for each asset.
    - For scraped data from a particular source (e.g., website), the copyright and terms of service of that source should be provided.
    - If assets are released, the license, copyright information, and terms of use in the package should be provided. For popular datasets, `paperswithcode.com/datasets` has curated licenses for some datasets. Their licensing guide can help determine the license of a dataset.

- For existing datasets that are re-packaged, both the original license and the license of the derived asset (if it has changed) should be provided.
- If this information is not available online, the authors are encouraged to reach out to the asset's creators.

13. **New Assets**

    Question: Are new assets introduced in the paper well documented and is the documentation provided alongside the assets?

    Answer: [NA]

    Justification: This paper does not release new assets.

    Guidelines:

    - The answer NA means that the paper does not release new assets.
    - Researchers should communicate the details of the dataset/code/model as part of their submissions via structured templates. This includes details about training, license, limitations, etc.
    - The paper should discuss whether and how consent was obtained from people whose asset is used.
    - At submission time, remember to anonymize your assets (if applicable). You can either create an anonymized URL or include an anonymized zip file.

14. **Crowdsourcing and Research with Human Subjects**

    Question: For crowdsourcing experiments and research with human subjects, does the paper include the full text of instructions given to participants and screenshots, if applicable, as well as details about compensation (if any)?

    Answer: [NA]

    Justification: This paper does not involve crowdsourcing nor research with human subjects.

    Guidelines:

    - The answer NA means that the paper does not involve crowdsourcing nor research with human subjects.
    - Including this information in the supplemental material is fine, but if the main contribution of the paper involves human subjects, then as much detail as possible should be included in the main paper.
    - According to the NeurIPS Code of Ethics, workers involved in data collection, curation, or other labor should be paid at least the minimum wage in the country of the data collector.

15. **Institutional Review Board (IRB) Approvals or Equivalent for Research with Human Subjects**

    Question: Does the paper describe potential risks incurred by study participants, whether such risks were disclosed to the subjects, and whether Institutional Review Board (IRB) approvals (or an equivalent approval/review based on the requirements of your country or institution) were obtained?

    Answer: [NA]

    Justification: This paper does not involve crowdsourcing nor research with human subjects.

    Guidelines:

    - The answer NA means that the paper does not involve crowdsourcing nor research with human subjects.
    - Depending on the country in which research is conducted, IRB approval (or equivalent) may be required for any human subjects research. If you obtained IRB approval, you should clearly state this in the paper.
    - We recognize that the procedures for this may vary significantly between institutions and locations, and we expect authors to adhere to the NeurIPS Code of Ethics and the guidelines for their institution.
    - For initial submissions, do not include any information that would break anonymity (if applicable), such as the institution conducting the review.